





Tunable quantum interference effects in Floquet two- and three-level systemsYingying Han ^{1,2} Minchen Qiao ^{3,4} Xiao-Qing Luo,⁵ Tie-Fu Li,^{6,7} Wenxian Zhang ³
Xiu-Hao Deng ^{1,8,*} J. Q. You,⁹ and Dapeng Yu^{1,8}¹*Shenzhen Institute for Quantum Science and Engineering, Southern University of Science and Technology, Shenzhen 518055, China*²*Shenzhen Key Laboratory of Ultraintense Laser and Advanced Material Technology, Center for Advanced Material Diagnostic Technology, and College of Engineering Physics, Shenzhen Technology University, Shenzhen 518118, China*³*Key Laboratory of Artificial Micro- and Nano-structures of Ministry of Education, and School of Physics and Technology, Wuhan University, Wuhan, Hubei 430072, China*⁴*School of integrated circuits, Tsinghua University, Beijing 100084, China*⁵*Hunan Province Key Laboratory for Ultra-Fast Micro/Nano Technology and Advanced Laser Manufacture, School of Electrical Engineering, University of South China, Hengyang 421001, China*⁶*School of Integrated Circuits and Frontier Science Center for Quantum Information, Tsinghua University, Beijing 100084, China*⁷*Beijing Academy of Quantum Information Sciences, Beijing 100193, China*⁸*Guangdong Provincial Key Laboratory of Quantum Science and Engineering, and Department of Physics, Southern University of Science and Technology, Shenzhen 518055, China*⁹*Interdisciplinary Center of Quantum Information, State Key Laboratory of Modern Optical Instrumentation, and Zhejiang Province Key Laboratory of Quantum Technology and Device, Department of Physics, Zhejiang University, Hangzhou 310027, China*

(Received 25 April 2022; accepted 13 June 2022; published 30 June 2022)

Quantum interference effects in the unmodulated quantum systems with light-matter interaction have been widely studied, such as electromagnetically induced transparency (EIT) and Autler-Townes splitting (ATS). However, the similar quantum interference effects in the Floquet systems (i.e., periodically modulated systems), which might cover rich new physics, were rarely studied. In this article, we investigate the quantum interference effects in the Floquet two- and three-level systems analytically and numerically. We show a coherent destruction tunneling effect in a lotuslike multipeak spectrum with a Floquet two-level system, where the intensity of the probe field is periodically modulated with a square-wave sequence. We demonstrate that the multipeak split into multiple transparency windows with tunable quantum interference if the Floquet system is asynchronously controlled via a third level. Based on phenomenological analysis with Akaike information criterion, we show that the symmetric central transparency window has a similar mechanism to the traditional ATS or EIT depending on the choice of parameters, additional with an extra degree of freedom to control the quantum interference provided by the modulation period. The other transparent windows are shown to be asymmetric, different from the traditional ATS and EIT windows. These nontrivial quantum interference effects open up a scope to explore the applications of the Floquet systems.

DOI: [10.1103/PhysRevA.105.063724](https://doi.org/10.1103/PhysRevA.105.063724)**I. INTRODUCTION**

Floquet systems, which could be characterized by periodically modulated Hamiltonian, display rich dynamics and novel phenomena that are absent in their unmodulated counterparts, such as quantum dynamical decoupling [1–3], time crystal [4,5], Mach-Zehnder interferometer [6,7], time-domain Fresnel lenses [8], time-domain grating [9], and Floquet topological phase [10]. The studies of periodically modulated systems are also known as Floquet engineering [11–15]. Moreover, for the Floquet systems, the dynamic

steady states are periodic steady states, which emerge in a balance of the energy injection by the periodic driving and the relaxation processes [16–18]. To explore the stability properties of the periodic steady states, the time-average values of observable physical quantities are usually observed experimentally [9,19] and stroboscopic evolution of a periodically driven quantum system in steps of the modulation period is usually adopted in theoretical studies [20].

Quantum interference effect (QIE) is the key to the quantum nature of a system. In an atom-field interacting quantum system, QIE enables rich interesting physics and applicable phenomena, such as electromagnetically induced transparency (EIT) [21,22] and Autler-Townes splitting (ATS) [23]. Both of them are observed with a transparency

*Corresponding email: dengxh@sustech.edu.cn

window induced by the unmodulated coherent drive fields, though they originate from controversial mechanisms that have been studied over decades in various systems and scenarios [24–26]. In the above unmodulated systems, the properties of QIE can be adjusted by manipulating the properties of the system, which is relatively difficult. Few studies have been done to alter the properties of QIE by using tunable auxiliary energy levels or phase-modulated fields [27–29]. Recently, with the rising interest in Floquet systems, rich novel physics are discovered, where the Floquet parameters (such as modulation period, modulation scheme, etc.) may be useful tools for tuning the properties of QIEs. However, to our knowledge, the QIEs in the Floquet controlled systems have not been adequately studied [30], especially the effect of the modulation period on the properties of QIEs.

In this work, we first study the Floquet two-level system, where the intensity of the probe field has the form of square-wave periodic sequence, which is a basic model of direct frequency comb spectroscopy [31] and is different from the sine and cosine pulse trains in the Mach-Zehnder interferometer [6,32]. Note that here the modulation period is shorter than the system's coherence time. We explore the steady excitation probability over a wide driving strength range and give the analytical results with some special scenarios. A lotuslike multipetale spectrum is observed and the coherent destruction of tunneling effect is found in the strong driving regime. When the Floquet two-level system assisted with a third energy level and a periodically modulated control field, each peak splits into two, resulting in multiple transparency windows. Here the modulation pulse of the control field is the same as that of the probe field, but they are asynchronous. An intriguing finding is that the central transparency window (CTW) in the Floquet three-level system has a similar profile to the traditional EIT or ATS in the un-modulated systems. We use the Akaike information criterion (AIC) method [33] to discern the CTW from EIT and ATS by evaluating their relative AIC weights for different modulation periods and find that the CTW could be EIT-like or ATS-like in different parameter regimes. Moreover, the quantum interference of the CTW can be modified by the modulation period, which as an additional degree of freedom increases the tunable space of CTW. Therefore, the CTW may provide a more superior platform for the explosion of quantum technology than the traditional EIT and ATS.

This work is outlined as follows. We explore the QIEs in the Floquet two-level system in Sec. II and Floquet three-level system in Sec. III. Conclusions and discussions are given in the last section of the article.

II. FLOQUET TWO-LEVEL SYSTEM

In this section, we first explore the QIEs in a Floquet two-level system denoted by $|0\rangle$ and $|1\rangle$ with energy $\omega_{0,1}$, as shown in Fig. 1(a). A probe field with frequency ω_p and periodically modulated Rabi frequency $\Omega_p(t) = \Omega_p(t + \tau)$ couples levels $|0\rangle$ and $|1\rangle$. Here τ is the modulation period and the detuning between the transition frequency (i.e., $\omega_{10} = \omega_1 - \omega_0$) and the frequency of the probe field is $\Delta = \omega_{10} - \omega_p$. To simplify the calculation, we consider the square-wave periodic sequence

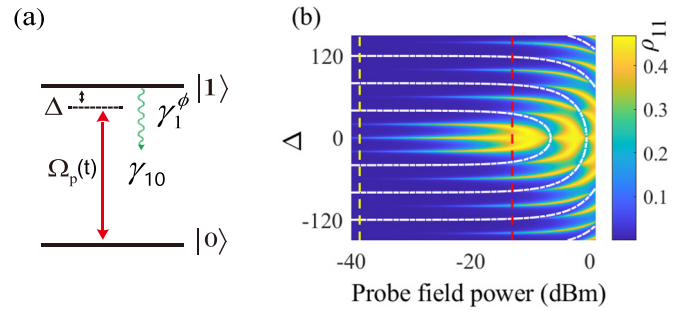


FIG. 1. (a) Schematic of a two-level system. A probe field couples levels $|0\rangle$ and $|1\rangle$ with a periodically modulated Rabi frequency $\Omega_p(t) = \Omega_p(t + \tau)$ and a detuning Δ . γ_{10} is the population damping rate from level $|1\rangle$ to $|0\rangle$. γ_1^ϕ is the dephasing rate of state $|1\rangle$. (b) The steady excitation probability ρ_{11} as a function of detuning and the probe field power. The graph is obtained by numerically calculating the Lindblad master equation in Eq. (3) for $\gamma_{10} = 1$, $\gamma_1^\phi = 0.4$, and $\tau = 0.05$. Note that in this work we normalized the parameters in terms of γ_{10} , such as $\gamma_1^\phi/\gamma_{10} = 0.4$, $\tau\gamma_{10} = 0.05$, and they are simplified to $\gamma_1^\phi = 0.4$ and $\tau = 0.05$. The white dashed lines show the excitation minima [i.e., $\sqrt{\Omega_p^2 + \Delta^2} = 2n\omega$ ($n = 1, 2, \dots$)] with modulation frequency $\omega = 1/\tau$. The vertical red dashed line at $\Omega_p = \omega = -13$ dBm divides the weak- and strong-coupling ranges. The vertical yellow dashed line denotes $\Omega_p = 1 \approx -38.6$ dBm.

as the modulation scheme in this work, i.e.,

$$\Omega_p(t) = \begin{cases} \Omega_p, & t \in [n\tau, (n + \frac{1}{2})\tau], \\ 0, & t \in [(n + \frac{1}{2})\tau, (n + 1)\tau], \end{cases} \quad (1)$$

with $n = 0, 1, 2, \dots$. The Hamiltonian of such a system is

$$H = \Delta(-|0\rangle\langle 0| + |1\rangle\langle 1|)/2 - [\Omega_p(t)|0\rangle\langle 1| + \text{H.c.}]/2, \quad (2)$$

with $\hbar = 1$. Note that, for our time-dependent Hamiltonian, here we apply the rotating-wave approximation (RWA) by assuming $\omega = 1/\tau \ll 2\omega_{10}$, $\Omega_p \ll \omega_{10}$, which are also the parameter ranges of many experimental studies. Our earlier experimental work has shown the validity of the RWA with a periodically driven superconducting qutrit [9]. Moreover, in Appendix A, we also theoretically verified the validity of RWA in detail. With the assumption of the Markovian noise background, the Floquet systems' density matrix evolves as the Lindblad master equation [34,35],

$$\dot{\rho} = -i[H(t), \rho] + \frac{\gamma_{10}}{2}(2\sigma_{01}\rho\sigma_{10} - \sigma_{11}\rho - \rho\sigma_{11}) + \gamma_1^\phi(2\sigma_{11}\rho\sigma_{11} - \sigma_{11}\rho - \rho\sigma_{11}), \quad (3)$$

where $\sigma_{ij} = |i\rangle\langle j|$ ($i, j = 0, 1$) are the projection operators and $H(t)$ is shown in Eq. (2). To observe the steady-state characteristics of the periodically driven systems, we only observe the data at the end of each modulation period (i.e., the time evolution step is τ), and ignore the microdynamics within one modulation period. The dynamics start from the ground state $|0\rangle$ and then evolve to the steady states (see also Fig. 5), which are observed to study the steady-state characteristics of the periodically driven systems.

Figure 1(b) shows the steady excitation probability ρ_{11} as a function of detuning and the probe field power. Note that here the unit of the probe field is dBm, where 1 dBm =

$10 \log(C \Omega_p^2)$, with $C = 1.38 \times 10^{-4}$ determined by experimental data [9,36]. We find a multipeak phenomenon in the weak driving range ($\Omega_p < -13$ dBm) and the sidebands are well separated, which is caused by the Fourier components of the square-wave modulated $\Omega_p(t)$ in Eq. (1), i.e.,

$$\Omega_p(t) = \frac{\Omega_p}{2} - \sum_{n=1}^{\infty} (-1)^n \Omega_{pn} \cos(\omega_n t), \quad (4)$$

where

$$\Omega_{pn} = \frac{\Omega_p}{(2n-1)\pi}, \quad (5)$$

$$\omega_n = (2n-1)\omega \quad (n = 1, 2, 3, \dots). \quad (6)$$

These expressions clearly demonstrate that the square-wave modulated field is equivalent to employing many frequency-tunable fields and the distance between them can be adjusted by the modulation frequency ω with frequency separation $\omega_{n+1} - \omega_n = 2\omega$.

In the strong driving range ($\Omega_p > -13$ dBm), the peaks get broader and overlap with each other, eventually forming a lotus pattern, which is too complex to get the analytic solution. However, we can obtain the steady solutions of ρ_{11} with $\Delta = 0$ by calculating the optical Bloch equations (see Appendix B),

$$\rho_{11} = \frac{1}{2} - \frac{\gamma_{10}}{2} \sum_{n=-\infty}^{\infty} \frac{\gamma_1 \Omega_n^2}{\gamma_1^2 + (\Omega_p/2 - n\omega)^2}, \quad (7)$$

where $\gamma_1 = 3\gamma_{10}/4 + \gamma_1^\phi/2$ and n are integers. Ω_n is a series of Bessel functions with variable Ω_p/ω [see Eq. (B15)]. When $\tau \rightarrow 0$, $\Omega_0 \rightarrow 1$, and $\Omega_{n \neq 0} \rightarrow 0$, then Eq. (7) can be reduced to $\rho_{11} \approx \frac{1}{2} - \frac{\gamma_{10}}{2} \frac{\gamma_1}{\gamma_1^2 + (\Omega_p/2)^2}$, which is close to the conventional result of the unmodulated system $\rho_{11} = \frac{1}{2} - \frac{\gamma_{10}}{2} \frac{\gamma_1'}{\gamma_1' \gamma_{10} + \Omega_p^2}$ with $\gamma_1' = \gamma_{10}/2 + \gamma_1^\phi$, except the effective Rabi frequency of the probe field to be $\Omega_p/2$. These indicate that, when $\tau \rightarrow 0$, the central peak of the multipeak phenomenon is similar to the single resonant peak in the unmodulated system. However, when τ away from 0, Ω_n significantly modifies the signal and induces a nontrivial phenomenon, coherent destruction of tunneling [37–39], where the steady excitation probability ρ_{11} is partially suppressed and arising from the superposition of degenerate Floquet states. When $\Delta = 0$, from Eq. (7) one finds that the conditions for ρ_{11} to take the local minimum values are $\Omega_p = 2n\omega$ ($n = 1, 2, \dots$). Expanding to the more general cases, the positions of the coherent destruction of tunneling are determined by the relationship between the effective Rabi frequency and the modulation frequency, i.e., $\sqrt{\Omega_p^2 + \Delta^2} = 2n\omega$ ($n = 1, 2, \dots$), as the white dashed lines shown in Fig. 1(b).

III. FLOQUET THREE-LEVEL SYSTEM

In this section, we further explore the QIEs in a Floquet three-level system, as shown in Fig. 2(a). Here we assume the modulation scheme of $\Omega_c(t)$ is asynchronous to that of

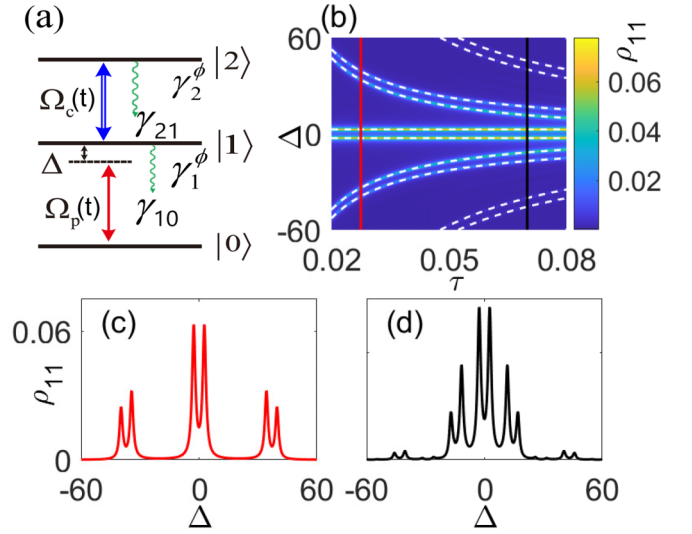


FIG. 2. (a) Schematic of a three-level system. Based on the above two-level system, a control field resonantly couples levels $|1\rangle$ and $|2\rangle$ with a periodically modulated Rabi frequency $\Omega_c(t) = \Omega_c(t + \tau)$. γ_{21} is the population damping rate from level $|2\rangle$ to $|1\rangle$. γ_2^ϕ is the dephasing rate of state $|2\rangle$. (b) A contour map of ρ_{11} as a function of Δ and τ . The graph is obtained by numerically calculating the Lindblad master equation (9) for $\gamma_{10} = 1$, $\gamma_{21} = 1.4$, $\gamma_1^\phi = 0.4$, $\gamma_1^\phi = 0.2$, $\Omega_c = 10.8$, and $\Omega_p = 1$ [i.e., the vertical yellow dashed line in Fig. 1(b)]. The white dashed lines show the positions of the resonance peaks, i.e., $(\Delta \pm \Omega_c/4)\tau = 2n\pi$ ($n = 0, 1, 2, \dots$). (c), (d) The steady excitation probability ρ_{11} as a function of the probe field detuning with $\tau = 0.027$ [i.e., the vertical red line in (b)] and $\tau = 0.695$ [i.e., the vertical black line in (b)]. Here we normalized the parameters in terms of γ_{10} .

$\Omega_p(t)$, i.e.,

$$\Omega_c(t) = \begin{cases} 0, & t \in [n\tau, (n + \frac{1}{2})\tau], \\ \Omega_c, & t \in [(n + \frac{1}{2})\tau, (n + 1)\tau], \end{cases} \quad (8)$$

with $n = 0, 1, 2, \dots$. Similar to the above two-level system, the Lindblad master equation can be written as

$$\begin{aligned} \dot{\rho} = & -i[H(t), \rho] + \sum_{j=1,2} \frac{\gamma_{j,j-1}}{2} \\ & \times (2\sigma_{j-1,j}\rho\sigma_{j,j-1} - \sigma_{jj}\rho - \rho\sigma_{jj}) \\ & + \sum_{j=1,2} \gamma_j^\phi (2\sigma_{jj}\rho\sigma_{jj} - \sigma_{jj}\rho - \rho\sigma_{jj}), \end{aligned} \quad (9)$$

with

$$\begin{aligned} H(t) = & \frac{\Delta}{2} (-|0\rangle\langle 0| + |1\rangle\langle 1| + |2\rangle\langle 2|) \\ & - \left[\frac{\Omega_p(t)}{2} |0\rangle\langle 1| + \frac{\Omega_c(t)}{2} |1\rangle\langle 2| + \text{H.c.} \right]. \end{aligned} \quad (10)$$

Similar to Eq. (2), here we apply RWA by assuming $\omega = 1/\tau \ll 2\omega_{10}, 2\omega_{21}, \Omega_p \ll \omega_{10}$, and $\Omega_c \ll \omega_{21}$.

To study the steady-state properties of the Floquet three-level system, only the data at the end of each modulation period (i.e., the time evolution step is τ) is observed. The dynamics start from the ground state $|0\rangle$; we show the contour map of ρ_{11} as a function of the probe field detuning Δ and

the modulation period τ in Fig. 2(b). One finds that each peak in Fig. 1(b) splits into two when an added control field couples $|1\rangle$ to $|2\rangle$, resulting in multiple transparency windows, which is similar to the multichromatic ATS with multitone control field studies in the unmodulated systems [40–42]. The positions of the peaks, as the white dashed lines shown in Fig. 2(b), could be demonstrated to be exactly the maximal constructive interference of transitions $|+\rangle \leftrightarrow |0\rangle$ and $|-\rangle \leftrightarrow |0\rangle$, which could be achieved by calculating relative phases $\phi_{0\pm}$ in one modulation period. Here $|\pm\rangle = (|2\rangle \pm |1\rangle)/\sqrt{2}$ is the dressed levels induced by the strong control field. During the controlled half period, the system is in the dressed basis $|\pm\rangle$ with eigenenergy $(\Delta \pm \Omega_c)/2$. The relative phases accumulated in the first half period are $\phi'_{0\pm} = (\Delta \pm \Omega_c/2)\tau/2$. During the noncontrolled half period, the system is in bare basis. Driven by a probe field with detuning Δ , the relative phases $\phi''_{0\pm}$ accumulated are $\phi''_{0+} = \phi''_{0-} \approx \Delta\tau/2$, where $\Omega_p \ll \Delta$ is assumed. Then the total relative phases in one period are $\phi_{0\pm} = \phi'_{0\pm} + \phi''_{0\pm} = (\Delta \pm \Omega_c/4)\tau$. The maximal interference requires $\phi_{0\pm} = 2n\pi$ ($n = 0, 1, 2, \dots$). Therefore, the constraints for absorption peaks are several curves $\Delta = 2n\pi\omega \pm \Omega_c/4$, as the white dashed lines shown in Fig. 2(b). The multiple transparency windows may have promising applications in quantum memory [43], ground-state cooling [44], and so on.

Figures 2(c) and 2(d) show the multiple transparency windows more clearly. One finds the asymmetry of the transparency windows except for the central one and the multiple transparency windows move closer to the center (i.e., $\Delta = 0$) as τ increases. Moreover, the central transparency window (CTW) is similar to the traditional EIT and ATS, but the modulation period as a new adjustable dimension enriches the interference properties of the CTW.

For the traditional EIT and ATS in the unmodulated systems, it is widely acknowledged that ATS exhibits a wide noninterference transparency window between large Stark splittings induced by a strong field [45,46], while EIT exhibits a narrow transparency window induced by destructive quantum interference (QI) between the Stark splittings [47]. In the weak probe field approximation, according to Ref. [48] the absorption of the probe field is determined by the first-order coherence of the probe transition and is given as

$$\text{Im}(\rho_{10})_{\text{QI}} = \frac{\Omega_p}{4B} \left[\left(\Delta - \frac{\Omega_c}{2} \right)^2 \Gamma + \left(\Delta + \frac{\Omega_c}{2} \right)^2 \Gamma + 2A \right], \quad (11)$$

where $A = -[(\frac{\Omega_c}{2})^2 - \Delta^2]\Lambda + (\Gamma - \Lambda)^2(\Gamma + \Lambda)$ and $B = [(\Delta + \frac{\Omega_c}{2})^2 + \Gamma^2][(\Delta - \frac{\Omega_c}{2})^2 + \Gamma^2] - 2[(\frac{\Omega_c}{2})^2 - \Delta^2 + \Gamma^2]\Lambda^2 + \Lambda^4$, with $\Gamma = (\gamma_{10} + \gamma_{21})/4 + (\gamma_1^\phi + \gamma_2^\phi)/2$ and $\Lambda = (\gamma_{10} - \gamma_{21})/4 + (\gamma_1^\phi - \gamma_2^\phi)/2$. Here Λ induces quantum interference between the transitions $|+\rangle \leftrightarrow |0\rangle$ and $|-\rangle \leftrightarrow |0\rangle$ (for more detail, see Appendix C). Then according to the well-known ATS (i.e., noninterference) [49], Λ should be zero and Eq. (11) reduces to

$$\text{Im}(\rho_{10})_{\text{ATS}} = \frac{\Gamma\Omega_p/4}{(\Delta - \frac{\Omega_c}{2})^2 + \Gamma^2} + \frac{\Gamma\Omega_p/4}{(\Delta + \frac{\Omega_c}{2})^2 + \Gamma^2}. \quad (12)$$

Equation (12) is exactly the sum of two Lorentzian peaks corresponding to transitions $|+\rangle \leftrightarrow |0\rangle$ and $|-\rangle \leftrightarrow |0\rangle$ with

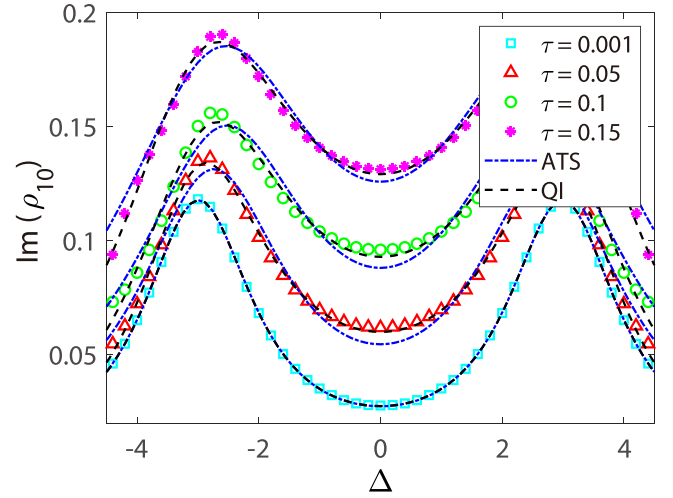


FIG. 3. Absorption $\text{Im}(\rho_{10})$ as a function of detuning Δ , and various τ with best fits to ATS ($\Omega_c, \Omega_p, \Gamma$) (black dashed lines) and QI ($\Omega_c, \Omega_p, \Gamma, \Lambda$) (blue dot dashed lines) models calculated for $\tau = 0.001$ (bright cyan squares) with a good fit to ATS (5.391, 0.4543, 0.9958) as well as QI (5.396, 0.4538, 0.9949, -0.0071), $\tau = 0.05$ (red triangles) with a better fit to QI (5.69, 0.56, 1.17, -0.73) than ATS (4.972, 0.6535, 1.326), $\tau = 0.1$ (green circles) with a better fit to QI (5.626, 0.7424, 1.447, -0.8687) than ATS (4.641, 0.8731, 1.607), and $\tau = 0.15$ (magenta asterisks) with a better fit to QI (5.847, 1.011, 1.657, -0.9817) than ATS (4.763, 1.231, 1.89). Here we normalized the parameters in terms of γ_{10} .

Stark splitting Ω_c . By comparing the values of $\text{Im}(\rho_{10})_{\text{ATS}}$ and $\text{Im}(\rho_{10})_{\text{QI}}$ in Eqs. (11) and (12) under $\Delta = 0$, we find that, when $0 < \Lambda < \Gamma$ ($-\Gamma < \Lambda < 0$), it induces destructive (constructive) interference and shallows (deepens) the absorption valley. Moreover, when $\Lambda \approx \Gamma$, absorption is almost completely suppressed [i.e., $\text{Im}(\rho_{10})_{\text{QI}}|_{\Delta=0} \approx 0$] due to complete destructive interference between transitions $|+\rangle \leftrightarrow |0\rangle$ and $|-\rangle \leftrightarrow |0\rangle$. Similarly, one has almost complete constructive interference for $\Lambda \approx -\Gamma$. When the control field is getting weaker or the decoherence rates are getting greater, the absorption dip corresponding to the transparency might disappear. Therefore, the additional condition for the probe transparency dip to be observed is $\partial \text{Im}(\rho_{10})_{\text{QI}}/\partial \Delta^2|_{\Delta=0} > 0$, giving $\Omega_c > 2\sqrt{(\Gamma - \Lambda)^3/(3\Gamma - \Lambda)}$.

To explore the interference properties of the CTW in our Floquet three-level system, the AIC method [33] is used to discern the CTW from QI and ATS models in Eqs. (11) and (12) by evaluating their relative AIC weights for different modulation periods.

A. ATS-like profile

In this section, we use the parameters that satisfy the ATS model in Eqs. (12), i.e., $\gamma_{10} = 1$, $\gamma_{21} = 1.4$, $\gamma_1^\phi = 0.4$, $\gamma_2^\phi = 0.2$, $\Omega_p = 1$, and $\Omega_c = 10.8$, which is also consistent with the parameters in Fig. 2. Then $\Gamma = 0.9$ and $\Lambda = 0$, where a noninterference transparency window appears for the unmodulated system. In Fig. 3, we plot the numerical results of $\text{Im}(\rho_{10})$ obtained from Eq. (9) for the Floquet three-level system. Note that here we only focus on the properties of the

CTW and the numerical results are obtained by calculating the dynamic steady states of the Floquet three-level system with time evolution step τ . As an objective way to identify the more appropriate model for the CTW in the Floquet three-level system, we also plot the fitting profile for each τ using QI ($\Omega_c, \Omega_p, \Gamma, \Lambda$) and ATS ($\Omega_c, \Omega_p, \Gamma$) models with fitting parameters $\Omega_p, \Omega_c, \Gamma$, and Λ in Eqs. (11) and (12) as a comparison. For small Floquet period, e.g., $\tau = 0.001$, ATS and QI fitting curves merge and both fit well with the simulated absorption. The fitted value of the interference term Λ is close to zero, which indicates that the CTW in a rapidly modulated system has similar properties to the transparency in its unmodulated counterparts. This could be understood as the quantum Zeno effect [50]. For larger Floquet periods, such as $\tau = 0.05, 0.1, 0.15$, we find that the CTW fits better with the QI model. The fitted interference $\Lambda < 0$, which indicates constructive interference in the CTW. This could be understood qualitatively as that the periodic driving heats the system and effectively changes the decay rates. However, as the modulation frequency ω increases, the heating speed becomes slower, which is known as Floquet prethermalization [51]. To conclude, in the ATS's parameter regime, the CTW is ATS-like but with significant interference adjustable in a wide range of modulation periods, which differentiates the CTW in the Floquet three-level system from the traditional ATS.

The above observations of the CTW's underlying mechanism are supported by quantitative criteria. To be specific, we apply the AIC method, which uses the relative entropy to identify the most informational model [45]. The information loss of a given model with k fitting parameters to the numerical data is quantified by $I = N \ln(R/N) + 2k$, where N is the number of numerical data for fitting and R denotes the fitting residual sum of squares. The per-point AIC contribution is $\bar{I} = I/N$. Hence the AIC per-point weights are

$$\bar{w}_{QI} = \frac{\exp(-\frac{1}{2}\bar{I}_{QI})}{\exp(-\frac{1}{2}\bar{I}_{ATS}) + \exp(-\frac{1}{2}\bar{I}_{QI})} \quad (13)$$

for the QI model and $\bar{w}_{ATS} = 1 - \bar{w}_{QI}$ for the ATS model. Greater weight means more likelihood of fitting. For $\tau = 0.001, 0.05, 0.1, 0.15$, $\bar{w}_{QI} = 0.51, 0.74, 0.75, 0.64$, respectively. Not surprisingly, for $\tau = 0.001$, $\bar{w}_{QI} \approx \bar{w}_{ATS}$. In general regions of τ , $\bar{w}_{QI} > \bar{w}_{ATS}$, which means that the QI model is indeed the more appropriate model for the CTW in the Floquet three-level system.

B. EIT-like profile

In this section, we further consider the parameters that satisfy the QI model in Eqs. (11), i.e., $\gamma_{10} = 1, \gamma_{21} = 0.1, \gamma_1^\phi = 3, \gamma_2^\phi = 0, \Omega_p = 1$, and $\Omega_c = 3.55$. Then $\Gamma = 1.775, \Lambda = 1.725$, which corresponds to almost completely destructive interference between transitions $|+\rangle \leftrightarrow |0\rangle$ and $|-\rangle \leftrightarrow |0\rangle$ under $\Delta = 0$. Similar to Sec. III A, Fig. 4 shows the numerical results of $\text{Im}(\rho_{10})$ and the fitting profile for each τ using the QI model in Eqs. (11). Note that here the poor ATS fitting results are ignored. When $\tau = 0.001$, the CTW has a narrow dip at zero detuning, which is similar to the conventional EIT in the unmodulated system. As the modulation period increases, the dip becomes shallow, and the modulation weakens

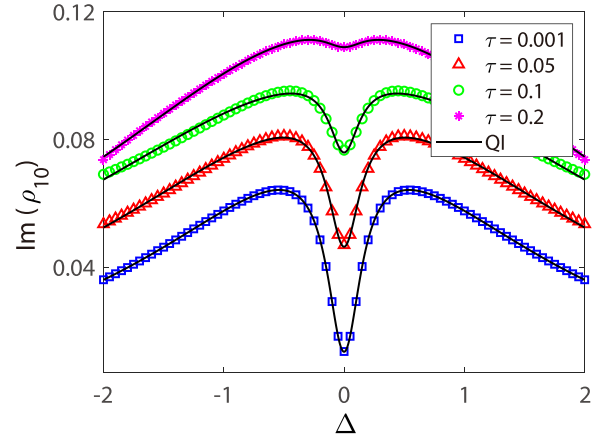


FIG. 4. Absorption $\text{Im}(\rho_{10})$ as a function of detuning Δ and various τ with best fits to QI ($\Omega_c, \Omega_p, \Gamma, \Lambda$) (black solid lines) model calculated for $\tau = 0.001, 0.05, 0.1, 0.2$ with a good fit to QI (0.4809, 1.812, 1.875, 1.817), QI (0.7392, 1.474, 2.31, 2.155), QI (1.018, 1.092, 2.736, 2.529), and QI(1.109, 0.5408, 2.62, 2.265), respectively. Here we normalized the parameters in terms of γ_{10} .

the strength of the destructive interference. Therefore, in the EIT parameter regime, the CTW is demonstrated to exhibit an EIT-like profile but with interference adjustable with the modulation period.

IV. DISCUSSIONS AND CONCLUSIONS

We investigate the QIEs in the Floquet two- and three-level systems. In the Floquet two-level system, the monochromatic periodic pulses (e.g., square wave) generate equivalent polychromatic drivings, which enable a lotuslike multipeak phenomenon and the coherent destruction of the tunneling effect. In the Floquet three-level system, where the probe and control fields are asynchronously modulated by the same square-wave pulses, multiple transparency windows are observed and the quantum interference of the CTW can be tuned by the modulation periods of the external fields. And the CTW becomes EIT-like or ATS-like by adjusting the modulation periods of the external fields without changing the properties of the systems, which will greatly improve the application prospects of the existing systems. Moreover, the multiple transparency windows may provide a powerful platform beyond the applications based on the traditional single transparent window, such as multifrequency all-optical switching, which can switch on and off multichromatic fields simultaneously.

The modulation scheme proposed here can be easily implemented experimentally in various three-level systems, such as atom gases [52,53], superconducting quantum circuits [54], quantum dots [55], nanoplasmonics [56], optomechanics [57,58], and so on. For a qutrit, which is a three-level artificial atom in the superconducting circuits, it can be manipulated by microwave fields. The modulation period τ that can be realized experimentally is about dozens of ns [9], which is much smaller than the coherence time of the system (about 0.5 ms) [59]. For such systems, hundreds of periods can be realized within the coherence time of the system.

ACKNOWLEDGMENTS

This work is supported by the National Natural Science Foundation of China under Grants No. U1930201, No. 91836101, No. U1801661, and No. 11934010, the Key-Area Research and Development Program of Guangdong Province (Grant No. 2018B030326001), Guangdong Provincial Key Laboratory (Grant No. 2019B121203002), the Science, Technology and Innovation Commission of Shenzhen Municipality (Grants No. JCYJ20170412152620376 and No. KYTDPT20181011104202253), Grant No. 2016ZT06D348, and the Natural Science Foundation of Guangdong Province (Grant No. 2017B030308003). X.-Q.L. acknowledges the support by the Foundation of Hunan Educational Committee (Grant No. 19C1585), the Natural Science Foundation of Hunan Province of China (Grant No. 2020JJ5466), and the National Natural Science Foundation of China (Grant No. 12104214).

APPENDIX A: VALIDITY OF ROTATING-WAVE APPROXIMATION FOR TIME-DEPENDENT HAMILTONIAN

In this section, we verify the validity of RWA with the Floquet two-level system described in the main text. The exact Hamiltonian is

$$H(t) = H_0 - \left[\frac{\Omega_p(t)(1 + e^{2i\omega_p t})}{2} |0\rangle\langle 1| + \text{H.c.} \right], \quad (\text{A1})$$

with $H_0 = \Delta(-|0\rangle\langle 0| + |1\rangle\langle 1|)/2$. Here $\exp(2i\omega_p t)$ is the counter-rotating term proportional to $\exp[\pm i(\omega_{10} + \omega_p - \Delta)t]$. Substituting Eq. (4) in the main text into Eq. (A1), the coupling term between levels $|0\rangle$ and $|1\rangle$ becomes

$$\left[\frac{\Omega_p}{2} - \sum_{n=1}^{\infty} (-1)^n \Omega_{pn} \cos(\omega_n t) \right] (1 + e^{2i\omega_p t}). \quad (\text{A2})$$

The counter-rotating term $\exp(2i\omega_p t)$ causes rotating terms proportional to $\exp[\pm i(\omega_n \pm 2\omega_p)t]$, which is usually a fast rotating term ($2\omega_p \gg \omega_n$) that can be ignored. For example, in superconducting circuit (atom) experiments, the frequency of the near-resonant microwave (laser) is several GHz (THz) [60,61]; however, the modulation frequency is about dozens of MHz [9]. Another condition for RWA to be applicable in Eq. (A2) is $\Omega_{pn} \ll \omega_n + \omega_p$, which can be simplified to $\Omega_p \ll \omega_p \approx \omega_{10}$, and this is the scenario we considered. Note that here we focus on the situation for small n , because the corresponding Rabi frequency Ω_{pn} decreases sharply as n increases. Therefore, in our Floquet system, the RWA is valid and, in ω_p 's rotating frame, Eq. (A1) becomes

$$H(t)_{\text{RWA}} = H_0 - \left[\frac{\Omega_p(t)}{2} |0\rangle\langle 1| + \text{H.c.} \right]. \quad (\text{A3})$$

In Fig. 5, we compare the numerical results of ρ_{11} obtained from Eq. (A1) and Eq. (A3) for the extensive parameters that we study in the main text, and find that the RWA results agree well with the exact results. Similarly, for our Floquet three-level system, the conditions for the RWA to be applicable are $\omega \ll 2\omega_{10}, 2\omega_{21}, \Omega_p \ll \omega_{10}$, and $\Omega_c \ll \omega_{21}$.

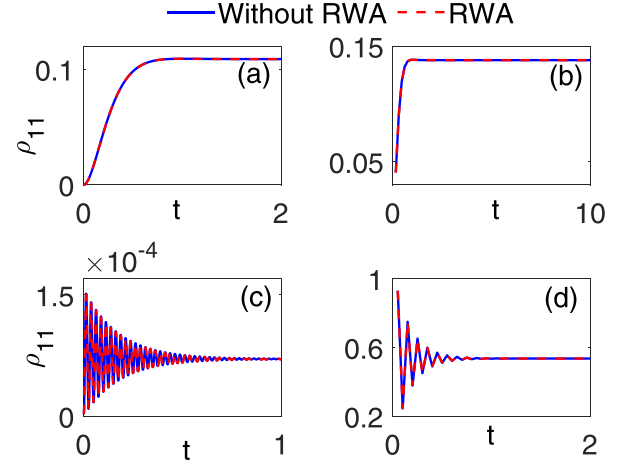


FIG. 5. Comparison of numerical results of ρ_{11} without RWA [obtained from Eq. (A1)] and with RWA [obtained from Eq. (A3)] for (a) $\tau = 0.001$, $\Delta = 0$, $\Omega_p = 1$, (b) $\tau = 0.15$, $\Delta = 0$, $\Omega_p = 1$, (c) $\tau = 0.001$, $\Delta = 40$, $\Omega_p = 1$, and (d) $\tau = 0.05$, $\Delta = 0$, $\Omega_p = 200$. Other parameters are $\omega_p = 6000$, $\omega_{10} = \Delta + \omega_p$, $\gamma_1^\phi = 0.4$, and $\gamma_{10} = 1$. Here we normalized the parameters in terms of γ_{10} .

APPENDIX B: ANALYTICAL RESULTS OF THE FLOQUET TWO-LEVEL SYSTEM

In the weak driving range ($\Omega_p < \omega$), the sidebands are well separated and show clearly resonance peaks caused by the different frequency components. The analytical results of these sidebands can be easily obtained as

$$\rho_{11} = \frac{\frac{\gamma_1'}{2\gamma_{10}} \left(\frac{\Omega_p}{2}\right)^2}{(\gamma_1')^2 + \Delta^2 + \frac{\gamma_1'}{\gamma_{10}} \left(\frac{\Omega_p}{2}\right)^2} + \sum_{n=1}^{\infty} \frac{\frac{\gamma_1'}{2\gamma_{10}} \Omega_{pn}^2}{(\gamma_1')^2 + (\Delta + \omega_n)^2 + \frac{\gamma_1'}{\gamma_{10}} \Omega_{pn}^2}, \quad (\text{B1})$$

with $\gamma_1' = \gamma_{10}/2 + \gamma_1^\phi$. Equation (B1) consists of a series of independent Lorentzians, each one with width $\sqrt{(\gamma_1')^2 + \gamma_1' \Omega_{pn}^2 / \gamma_{10}}$.

In the strong driving range ($\Omega_p > \omega$), the pattern becomes too complex to get the analytic solution. However, we can get the analytical expression for the resonance condition ($\Delta = 0$) and expand to the general case. When $\Delta = 0$, the optical Bloch equations are

$$\frac{\partial V(t)}{\partial t} = -\gamma_1' V, \quad (\text{B2})$$

$$\begin{aligned} \frac{\partial U(t)}{\partial t} &= \frac{\gamma_{10}}{2} - \frac{1}{2}(\gamma_{10} + \gamma_1')U(t) + i\Omega_p(t)U(t) \\ &\quad - \frac{1}{2}(\gamma_{10} - \gamma_1')W(t), \end{aligned} \quad (\text{B3})$$

$$\begin{aligned} \frac{\partial W(t)}{\partial t} &= \frac{\gamma_{10}}{2} - \frac{1}{2}(\gamma_{10} + \gamma_1')W(t) - i\Omega_p(t)W(t) \\ &\quad - \frac{1}{2}(\gamma_{10} - \gamma_1')U(t), \end{aligned} \quad (\text{B4})$$

where

$$V(t) = \frac{1}{2}[\rho_{10}(t) + \rho_{01}(t)], \quad (\text{B5})$$

$$U(t) = \frac{1}{2}[\rho_{11}(t) - \rho_{00}(t) + \rho_{01}(t) - \rho_{10}(t)], \quad (\text{B6})$$

$$W(t) = \frac{1}{2}[\rho_{11}(t) - \rho_{00}(t) - \rho_{01}(t) + \rho_{10}(t)]. \quad (\text{B7})$$

In the absence of damping ($\gamma_{10} = \gamma'_1 = 0$), the solutions of Eqs. (B3) and (B4) show that the components $U(t)$ and $W(t)$ oscillate with frequencies $\pm\Omega_p(t)$, and their oscillation frequencies differ by $2\Omega_p(t)$. Therefore, in a frame oscillating with $\Omega_p(t)$ the terms proportional to $(\gamma_{10} - \gamma'_1)/2$ oscillate with $\pm 2\Omega_p(t)$. Thus we can ignore the rapidly oscillating terms and obtain the solutions of $U(t)$ and $W(t)$ by direct integration [62],

$$U(t) = -\frac{\gamma_{10}}{2} \int_0^t dt' e^{iA(t-t')} e^{\sum_{n=1}^{\infty} B[\sin(\omega_n t') - \sin(\omega_n t)]}, \quad (\text{B8})$$

where

$$A = -\frac{1}{2}(\gamma_{10} + \gamma'_1 - i\Omega_p), \quad B = \frac{i(-1)^{n+1}\Omega_{pn}}{\omega_n}. \quad (\text{B9})$$

It is seen from Eq. (B6) that

$$\frac{\rho_{11}(t) - \rho_{00}(t)}{2} = \text{Re}[U(t)]. \quad (\text{B10})$$

Combined with $\rho_{11}(t) + \rho_{00}(t) = 1$, the population of state $|1\rangle$ is

$$\rho_{11}(t) = \frac{1}{2} - \text{Re}[U(t)]. \quad (\text{B11})$$

From Eq. (B6), we also get

$$\text{Im}[\rho_{10}(t)] = -\text{Im}[U(t)]. \quad (\text{B12})$$

Substituting Eq. (B8) into Eq. (B11) and Eq. (B12), and straightforward calculating the steady solution of ρ_{11} and $\text{Im}(\rho_{10})$

$$\rho_{11}(\infty) = \frac{1}{2} - \frac{\gamma_{10}\gamma_1}{2} \sum_{n=-\infty}^{\infty} \frac{\Omega_n^2}{\gamma_1^2 + (\Omega_p/2 - n\omega)^2}, \quad (\text{B13})$$

$$\text{Im}[\rho_{10}(\infty)] = \frac{\gamma_{10}}{2} \sum_{n=-\infty}^{\infty} \frac{\Omega_n^2(\Omega_p/2 - n\omega)}{\gamma_1^2 + (\Omega_p/2 - n\omega)^2}, \quad (\text{B14})$$

where

$$\begin{aligned} \Omega_n &= \sum_{\xi=-\infty}^{\infty} \sum_{l=-\infty}^{\infty} \cdots \sum_{g=-\infty}^{\infty} J_{\xi} \left(\frac{-2\Omega_p}{\omega\pi} \right) J_l \left(\frac{2\Omega_p}{9\omega\pi} \right) \cdots \\ &\times J_g \left(\frac{(-1)^g 2\Omega_p}{(2q-1)^2 \omega\pi} \right), \end{aligned} \quad (\text{B15})$$

with $\xi = n - 3l - \cdots - (2q-1)g$ and $\gamma_1 = (\gamma'_1 + \gamma_{10})/2$. From Eqs. (B13)–(B15), we find that the steady solutions of ρ_{11} and $\text{Im}(\rho_{10})$ are related with Ω_n^2 , which is a series of Bessel functions with variable Ω_p/ω . In Fig. 6, we plot $(\Omega_n)^2$ as a function of τ with $\Omega_p = 1$ and find that only $\Omega_0^2 \neq 0$, when $\tau \rightarrow 0$.

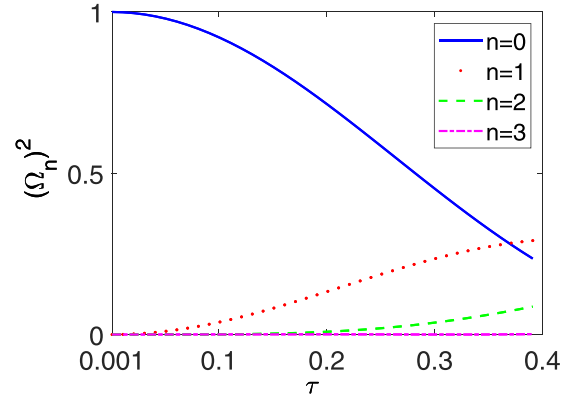


FIG. 6. $(\Omega_n)^2$ [obtained from Eq. (B15)] as a function of τ with $\Omega_p = 1$. Here we normalized the parameters in terms of γ_{10} .

APPENDIX C: DERIVATION OF QI AND ATS MODELS IN EQS. (11) AND (12)

In this section, we derive the QI and ATS models in Eqs. (11) and (12) with an unmodulated Hamiltonian

$$\begin{aligned} H &= \frac{\Delta}{2} (|1\rangle\langle 1| + |2\rangle\langle 2| - |0\rangle\langle 0|) \\ &- \left(\frac{\Omega_p}{2} |0\rangle\langle 1| + \frac{\Omega_c}{2} |1\rangle\langle 2| + \text{H.c.} \right). \end{aligned} \quad (\text{C1})$$

The dynamics affected by the control field could be better studied in dressed state representation by replacing the $H(t)$ in Eq. (9) with Eq. (C1) [48]. The elements in the density matrix associated with the probed transition dynamics are

$$\begin{aligned} \dot{\rho}_{-0} &= - \left[i \left(\Delta + \frac{\Omega_c}{2} \right) + \Gamma \right] \rho_{-0} - \Lambda \rho_{+0} \\ &+ \frac{i\Omega_p}{2\sqrt{2}} (\rho_{00} - \rho_{--} - \rho_{+-}), \end{aligned} \quad (\text{C2})$$

$$\begin{aligned} \dot{\rho}_{+0} &= - \left[i \left(\Delta - \frac{\Omega_c}{2} \right) + \Gamma \right] \rho_{+0} - \Lambda \rho_{-0} \\ &+ \frac{i\Omega_p}{2\sqrt{2}} (\rho_{00} - \rho_{++} - \rho_{+-}). \end{aligned} \quad (\text{C3})$$

From Eqs. (C2) and (C3), one finds that Λ cross couples the two dressed states' dynamics and induces quantum interference between ρ_{+0} and ρ_{-0} . Then we give the first-order steady solutions of ρ_{+0} and ρ_{-0} with the weak probe field approximation, where the steady-state zero-order populations and coherence are $\rho_{00}^0 = 1$, $\rho_{++}^0 = \rho_{--}^0 = \rho_{+-}^0 = 0$. With these conditions, Eqs. (C2) and (C3) become

$$\dot{\rho}_{-0} = - \left[i \left(\Delta + \frac{\Omega_c}{2} \right) + \Gamma \right] \rho_{-0} - \Lambda \rho_{+0} + \frac{i\Omega_p}{2\sqrt{2}}, \quad (\text{C4})$$

$$\dot{\rho}_{+0} = - \left[i \left(\Delta - \frac{\Omega_c}{2} \right) + \Gamma \right] \rho_{+0} - \Lambda \rho_{-0} + \frac{i\Omega_p}{2\sqrt{2}}. \quad (\text{C5})$$

This set of equations can be solved by writing in the matrix form,

$$\dot{R} = -MR + A, \quad (\text{C6})$$

with

$$R = \begin{pmatrix} \rho_{-0} \\ \rho_{+0} \end{pmatrix}, \quad (\text{C7})$$

$$M = \begin{pmatrix} i(\Delta + \frac{\Omega_c}{2}) + \Gamma & \\ & i(\Delta - \frac{\Omega_c}{2}) + \Gamma \end{pmatrix}, \quad (\text{C8})$$

$$A = \begin{pmatrix} \frac{i\Omega_p}{2\sqrt{2}} \\ \frac{i\Omega_p}{2\sqrt{2}} \end{pmatrix}, \quad (\text{C9})$$

and then integrating

$$R(t) = \int_{-\infty}^t e^{-M(t-t')A} dt' = M^{-1}A. \quad (\text{C10})$$

This yields

$$\rho_{-0} = \frac{i\Omega_p}{2\sqrt{2}} \frac{i(\Delta - \frac{\Omega_c}{2}) + \Gamma - \Lambda}{[i(-\Delta - \frac{\Omega_c}{2}) - \Gamma][i(-\Delta + \frac{\Omega_c}{2}) - \Gamma] - \Lambda^2}, \quad (\text{C11})$$

$$\rho_{+0} = \frac{i\Omega_p}{2\sqrt{2}} \frac{i(\Delta + \frac{\Omega_c}{2}) + \Gamma - \Lambda}{[i(-\Delta - \frac{\Omega_c}{2}) - \Gamma][i(-\Delta + \frac{\Omega_c}{2}) - \Gamma] - \Lambda^2}. \quad (\text{C12})$$

Then the absorption of the probe field is $\text{Im}(\rho_{10}) = \text{Im}(\rho_{+0} + \rho_{-0})/\sqrt{2}$.

-
- [1] J. Jing, L.-A. Wu, M. Byrd, J. Q. You, T. Yu, and Z.-M. Wang, *Phys. Rev. Lett.* **114**, 190502 (2015).
- [2] W. Zhang, V. V. Dobrovitski, L. F. Santos, L. Viola, and B. N. Harmon, *Phys. Rev. B* **75**, 201302(R) (2007).
- [3] W. Zhang, N. P. Konstantinidis, V. V. Dobrovitski, B. N. Harmon, L. F. Santos, and L. Viola, *Phys. Rev. B* **77**, 125336 (2008).
- [4] D. V. Else, B. Bauer, and C. Nayak, *Phys. Rev. Lett.* **117**, 090402 (2016).
- [5] K. Sacha and J. Zakrzewski, *Rep. Prog. Phys.* **81**, 016401 (2018).
- [6] W. D. Oliver, Y. Yu, J. C. Lee, K. K. Berggren, L. S. Levitov, and T. P. Orlando, *Science* **310**, 1653 (2005).
- [7] S. Shevchenko, S. Ashhab, and F. Nori, *Phys. Rep.* **492**, 1 (2010).
- [8] J. Degert, W. Wohlleben, B. Chatel, M. Motzkus, and B. Girard, *Phys. Rev. Lett.* **89**, 203003 (2002).
- [9] Y. Han, X.-Q. Luo, T.-F. Li, W. Zhang, S.-P. Wang, J. S. Tsai, F. Nori, and J. Q. You, *Phys. Rev. Appl.* **11**, 014053 (2019).
- [10] H. Wu and J.-H. An, *Phys. Rev. B* **102**, 041119(R) (2020).
- [11] M. Bukov, L. D'Alessio, and A. Polkovnikov, *Adv. Phys.* **64**, 139 (2014).
- [12] W.-L. Song, J.-B. You, J. K. Xu, W. L. Yang, and J.-H. An, *Phys. Rev. Appl.* **14**, 054049 (2020).
- [13] X. Luo, Q. Xie, and B. Wu, *Phys. Rev. A* **77**, 053601 (2008).
- [14] Z.-Y. Zeng, L. Li, B. Yang, J. Xiao, and X. Luo, *Phys. Rev. A* **102**, 012221 (2020).
- [15] Y. Han, X.-Q. Luo, T.-F. Li, and W. Zhang, *Phys. Rev. A* **101**, 022108 (2020).
- [16] V. I. Yudin, A. V. Taichenachev, and M. Y. Basalaeu, *Phys. Rev. A* **93**, 013820 (2016).
- [17] T. N. Ikeda and M. Sato, *Sci. Adv.* **6**, eabb4019 (2020).
- [18] Y. Han, W. Zhang, and W. Li, *Opt. Express* **30**, 7987 (2022).
- [19] C. Ying, Q. Guo, S. Li, M. Gong, X.-H. Deng, F. Chen, C. Zha, Y. Ye, C. Wang, Q. Zhu *et al.*, *Phys. Rev. A* **105**, 012418 (2022).
- [20] C. M. Dai, Z. C. Shi, and X. X. Yi, *Phys. Rev. A* **93**, 032121 (2016).
- [21] S. E. Harris, J. E. Field, and A. Imamoglu, *Phys. Rev. Lett.* **64**, 1107 (1990).
- [22] H. Ian, Y.-x. Liu, and F. Nori, *Phys. Rev. A* **81**, 063823 (2010).
- [23] S. H. Autler and C. H. Townes, *Phys. Rev.* **100**, 703 (1955).
- [24] Y. Zhang, P. Li, H. Zheng, Z. Wang, H. Chen, C. Li, R. Zhang, and M. Xiao, *Opt. Express* **19**, 7769 (2011).
- [25] T. Y. Abi-Salloum, *Phys. Rev. A* **81**, 053836 (2010).
- [26] C. Zhu, C. Tan, and G. Huang, *Phys. Rev. A* **87**, 043813 (2013).
- [27] H.-C. Sun, Y.-x. Liu, H. Ian, J. Q. You, E. Il'ichev, and F. Nori, *Phys. Rev. A* **89**, 063822 (2014).
- [28] W. Zhao, Y. Zhang, and Z. Wang, *Front. Phys.* **17**, 42506 (2022).
- [29] H. Wanare, *Phys. Rev. Lett.* **96**, 183601 (2006).
- [30] M. Holthaus and B. Just, *Phys. Rev. A* **49**, 1950 (1994).
- [31] N. Picque and T. W. Hansch, *Nat. Photon.* **13**, 146 (2019).
- [32] X. Tan, D.-W. Zhang, Z. Zhang, Y. Yu, S. Han, and S.-L. Zhu, *Phys. Rev. Lett.* **112**, 027001 (2014).
- [33] P. M. Anisimov, J. P. Dowling, and B. C. Sanders, *Phys. Rev. Lett.* **107**, 163604 (2011).
- [34] A. Schnell, S. Denisov, and A. Eckardt, *Phys. Rev. B* **104**, 165414 (2021).
- [35] A. Schnell, A. Eckardt, and S. Denisov, *Phys. Rev. B* **101**, 100301(R) (2020).
- [36] Q.-C. Liu, T.-F. Li, X.-Q. Luo, H. Zhao, W. Xiong, Y.-S. Zhang, Z. Chen, J. S. Liu, W. Chen, F. Nori *et al.*, *Phys. Rev. A* **93**, 053838 (2016).
- [37] F. Grossmann, T. Dittrich, P. Jung, and P. Hänggi, *Phys. Rev. Lett.* **67**, 516 (1991).
- [38] S. Ashhab, J. R. Johansson, A. M. Zagoskin, and F. Nori, *Phys. Rev. A* **75**, 063414 (2007).
- [39] L. Li, X. Luo, X.-Y. Lü, X. Yang, and Y. Wu, *Phys. Rev. A* **91**, 063804 (2015).
- [40] X. M. Hu, Q. Xu, J. Y. Li, X. X. Li, W. X. Shi, and X. Zhang, *Opt. Commun.* **260**, 196 (2006).
- [41] M. Jakob and G. Y. Kryuchkyan, *Phys. Rev. A* **57**, 1355 (1998).
- [42] J. Wang, Y. Zhu, K. J. Jiang, and M. S. Zhan, *Phys. Rev. A* **68**, 063810 (2003).
- [43] Y.-F. Hsiao, P.-J. Tsai, H.-S. Chen, S.-X. Lin, C.-C. Hung, C.-H. Lee, Y.-H. Chen, Y.-F. Chen, I. A. Yu, and Y.-C. Chen, *Phys. Rev. Lett.* **120**, 183602 (2018).
- [44] Z. Yi, W.-j. Gu, and G.-x. Li, *Opt. Express* **21**, 3445 (2013).
- [45] B. Peng, Ö. SK, W. Chen, F. Nori, and L. Yang, *Nat. Commun.* **5**, 5082 (2014).
- [46] L.-Y. He, T.-J. Wang, Y.-P. Gao, C. Cao, and C. Wang, *Opt. Express* **23**, 23817 (2015).

- [47] M. Fleischhauer, A. Imamoglu, and J. P. Marangos, *Rev. Mod. Phys.* **77**, 633 (2005).
- [48] S. Davuluri and S. Zhu, *Phys. Scr.* **91**, 013008 (2016).
- [49] J. Liu, J. Wu, Y. Zhang, Y. He, and J. Zhang, *J. Opt. Soc. Am. B* **37**, 49 (2020).
- [50] W. M. Itano, D. J. Heinzen, J. J. Bollinger, and D. J. Wineland, *Phys. Rev. A* **41**, 2295 (1990).
- [51] A. Rubio-Abadal, M. Ippoliti, S. Hollerith, D. Wei, J. Rui, S. L. Sondhi, V. Khemani, C. Gross, and I. Bloch, *Phys. Rev. X* **10**, 021044 (2020).
- [52] M. D. Lukin, M. Fleischhauer, A. S. Zibrov, H. G. Robinson, V. L. Velichansky, L. Hollberg, and M. O. Scully, *Phys. Rev. Lett.* **79**, 2959 (1997).
- [53] I. Novikova, R. Walsworth, and Y. Xiao, *Laser Photon. Rev.* **6**, 333 (2012).
- [54] J. Q. You and F. Nori, *Nature (London)* **474**, 589 (2011).
- [55] X. Xu, B. Sun, P. R. Berman, D. G. Steel, A. S. Bracker, D. Gammon, and L. J. Sham, *Science* **317**, 929 (2007).
- [56] N. Liu, L. Langguth, T. Weiss, J. Kästel, M. Fleischhauer, T. Pfau, and H. Giessen, *Nat. Mater.* **8**, 758 (2009).
- [57] A. H. Safavi-Naeini, T. P. M. Alegre, J. Chan, M. Eichenfield, M. Winger, Q. Lin, J. T. Hill, D. E. Chang, and O. Painter, *Nature (London)* **472**, 69 (2011).
- [58] C. Jiang, H. Liu, Y. Cui, X. Li, G. Chen, and B. Chen, *Opt. Express* **21**, 12165 (2013).
- [59] C. Wang, X. Li, H. Xu, Z. Li, J. Wang, Z. Yang, Z. Mi, X. Liang, T. Su, C. Yang *et al.*, *npj Quantum Inf.* **8**, 3 (2022).
- [60] H. Paik, D. I. Schuster, L. S. Bishop, G. Kirchmair, G. Catelani, A. P. Sears, B. R. Johnson, M. J. Reagor, L. Frunzio, L. I. Glazman *et al.*, *Phys. Rev. Lett.* **107**, 240501 (2011).
- [61] C. Rigetti, J. M. Gambetta, S. Poletto, B. L. T. Plourde, J. M. Chow, A. D. Córcoles, J. A. Smolin, S. T. Merkel, J. R. Rozen, G. A. Keefe *et al.*, *Phys. Rev. B* **86**, 100506(R) (2012).
- [62] Z. Ficek, J. Seke, A. Soldatov, and G. Adam, *J. Opt. B* **2**, 780 (2000).